Distance and Velocity Characterizations Through Sampling Rate-Limited Main Interferometer in a Silicon Platform

Ting-Qing Liao, Ting-Chia Chang, Jhih-Jia Kang, and Shih-Hsiang Hsu

***Abstract*—The Hilbert transform can resample the signal to compensate for the nonlinear frequency sweeping phenomenon and precisely measure a distance and velocity through frequency-modulated continuous-wave (FMCW). Instead of an additional auxiliary interferometer, the direct Hilbert-transform resampling on the main interferograms of a silicon platform could correct the optical-source phase error to form compact light detection and ranging (LiDAR) systems in the characterizations of distances and velocities. More than two samples in an interferogram period will be a criterion in the sampling rate-limited FMCW distance tests. 876.86 cm and 18.058 cm ranging limits are demonstrated through 5×10^5 and $1x10^4$ samples per second from the data acquisition, respectively, in a process-insensitive Mach-Zehnder directional coupler for FMCW-based LiDAR applications. The velocity of 200 mm per second was also illustrated in 5×10^5 samples per second. Moreover, the Hilbert-transform resampled on the main interferometer is superior to the peak-valley approach in the resampling data points, ranging accuracy, and low noise.**

***Index Terms*—FMCW, LiDAR, resampling, Hilbert transform, auxiliary interferometer, main interferometer.**

I. Introduction

LIGHT detection and ranging (LiDAR) is a technology that can measure the distance and speed of a target in addition to image acquisition. It has been growing and advancing rapidly in autonomous driving, drone navigation, and safety monitoring, bringing convenience and security to our lives. LiDAR can provide more information and make the related applications more diversified and active.

Currently, two main types of light detection and ranging (LiDAR) are prevalent: Time of Flight (ToF) and Frequency-Modulated Continuous-Wave (FMCW). FMCW LiDAR offers better details in measuring distances, can handle environmental noise better, and has improved distance detection capabilities compared to ToF LiDAR. In the nonlinear optical source outputs in Fourier-domain-based systems such as spectral-domain optical coherence tomography (SD-OCT), swept-source OCT (SS-OCT), optical frequency-domain reflectometry (OFDR), and LiDAR, resampling techniques are widely employed for correction in spectrometer in k space [1], dispersion compensation [2], laser swept-rate linearization [3], and amplitude modulation [4]. This paper will demonstrate and implement a software-assisted technique to linearize the swept laser's nonlinear frequency for interference phase error emendations in FMCW LiDAR velocity and distance measurements.

Optoelectronic integrated circuit technology, especially silicon photonics integrated circuits, is a crucial solution for supporting next-generation applications in communication, artificial intelligence, optical sensing, and more. Optoelectronic chips, leveraging advantages like miniaturization, energy efficiency, and cost-effective mass production, are a primary choice for leading information technology companies to develop chip-level high-speed signal transmission.

To mitigate the laser nonlinearity effects, the Hilbert transform [5], extreme points [6], equispaced phase [7], and phase lock loop (PLL) [8] were employed in the auxiliary interferometer for resampling. However, the FMCW LiDAR velocity test experiments illustrate that the significant vibrations generated by the stepping motor result in different instantaneous frequency variations between the static and dynamic coordinate systems. Consequently, using auxiliary interferometers for resampling to measure objects in high velocities is not feasible. We propose to utilize the main interferometer in resampling for FMCW in velocity and range tests.

The optical coupler is the crucial component for the LiDAR. The Mach-Zehnder direction coupler (MZDC) is used to replace the directional coupler (DC) because it owns the wavelength insensitivity in the power divider [9]. The flat wavelength response could faithfully transfer the wavelength response [10] from the swept light source.

The previous studies used the Hilbert transformation and extreme points in the auxiliary interferometer to correct the nonlinear phases from the swept source. In LiDAR applications, the auxiliary interferometer-based resample requires the optical path difference (OPD) to be at least twice the measured distance to meet the Nyquist theorem, impractical for the FMCW applications in a silicon platform. For the main interferometer-based

Manuscript received 1 December 2023; revised 2 May 2024; accepted 9 May 2024. Date of publication 16 May 2024; date of current version 23 May 2024. This work was supported in part by the National Science and Technology Council (Ministry of Science and Technology (MOST)) of the Republic of China under Grant MOST 110-2221-E-011-107 and Grant NSTC 111-2221-E-011-053 and in part by the Heterogeneously-integrated Silicon Photonic Integration Center of National Taiwan University of Science and Technology. *(Corresponding author: Shih-Hsiang Hsu.)*

The authors are with the Department of Electronics and Computer Engineering, National Taiwan University of Science and Technology, Taipei 106335, Taiwan (e-mail: m11102333@mail.ntust.edu.tw; m11102312@mail.ntust.edu.tw; m10819004@mail.ntust.edu.tw; shsu@mail.ntust.edu.tw).

Digital Object Identifier 10.1109/JPHOT.2024.3401550

resampling, the Hilbert transformation and extreme points will be studied and compared for the accuracy and signal-to-noise ratios in FMCW ranging and speeds.

Moreover, the interferograms from the main interferometer will go through the Fourier transform for the FMCW-related information. The scan wavelength range of the swept source is incorporated with the sampling rate of the data acquisition (DAQ) for each period of interference. Too few points in DAQ cannot represent comprehensive and sophisticated interferograms for the FMCW-based velocity and range. The experiments will be conducted to compare and investigate the effect of the sample number in one interferogram period in terms of distance and velocities. The Hilbert transform was used to extract the non-linear phases of the main interference signals and restore the wavelength points corresponding to each interferogram phase interval. For a distance of 24 cm, we demonstrated the velocity measurements on the main interferometer-based Hilbert transform. The sampling rate-limited ranging tests will be shown on half of one mega-sample per second through the main interferometer-based Hilbert-transform resampling.

II. Theory and Simulation

The electric field of the main interferometer signal can be represented in the following:

$$E_{main}(t) = A_m \sin\left[\varphi(t) - \varphi(t-\tau) + \varphi_0\right] \tag{1}$$

where A_m is the amplitude of the electric field of the main interference, and τ is the time delay. $\varphi(t)$ and $\varphi(t-\tau)$ are the signal phase and reference phase, respectively. φ_0 is the constant phase. After the higher-order terms in Taylor's expression of the phase are negligible, the main interference phase difference can be written as follows:

The beat frequency used for the experimental distance and velocity calculations can be expressed as follows:

$$\varphi(t) - \varphi(t-\tau) = \tau\frac{d\varphi(t)}{dt} = \tau 2\pi f(t) \tag{2}$$

Then

$$E_{main}(t) = A_m \sin\left[2\pi\tau f(t) + \varphi_0\right] \tag{3}$$

where $f(t)$ is the frequency tuning rate.

After the Hilbert transformation, the imaginary parts of the main interferometer signal can be listed as follows:

$$Hilbert\left[E_{main}(t)\right] = A_m \cos\left[2\pi\tau f(t) + \varphi_0\right] \tag{4}$$

$$f(\mathrm{t}) = \frac{1}{2\pi\tau}\left(\tan^{-1}\left\{\frac{E_{main}(t)}{\mathrm{Hilbert}\left[E_{main}(t)\right]}\right\} - \varphi_0\right)$$
$$= \frac{1}{2\pi \mathrm{n}}\frac{\mathrm{c}}{\Delta \mathrm{L}}\left(\tan^{-1}\left\{\frac{E_{main}(t)}{\mathrm{Hilbery}\left[E_{main}(t)\right]}\right\} - \varphi_0\right) \tag{5}$$

where n and ΔL are the refractive index and optical path difference between the reference and signal parts, respectively. c is the light velocity.

There are two beat frequencies when the triangular modulation is applied to the interferometer system. The Doppler frequency, f_{doppler}, used to calculate the velocity can be obtained from the following equation:

$$f_{\mathrm{doppler}} = \frac{1}{2}\left(f_{\mathrm{beat}}(down) + f_{\mathrm{beat}}(up)\right) \tag{6}$$

where $f_{\mathrm{beat}}(up)$ represents the higher beat frequency in the triangular modulation, and $f_{\mathrm{beat}}(down)$ is the lower one.

The Hilbert transform is a mathematical tool for obtaining the instantaneous phase of a signal from its amplitude or envelope. In the context of optical power, it can be used to extract the phase information from the optical intensity signal [5]. Therefore, the instantaneous frequency can be obtained by converting the immediate phase, and the average velocity $\mathrm{V_{ave}}$ can be calculated in the following:

$$\mathrm{V_{ave}} = \frac{\mathrm{C}}{4f_0} f_{\mathrm{doppler}} = \frac{\lambda_0}{4} f_{\mathrm{doppler}} \tag{7}$$

where f_0 and λ_0 are the initial frequency and wavelength of the laser, respectively. c is the light velocity.

As for the distance tests, the sawtooth modulation is used to derive the beat frequency as follows:

$$f_{\mathrm{beat}} = \frac{2Bn_g\Delta L}{TC} \tag{8}$$

where T and B are the sawtooth modulation period and bandwidth, respectively. ΔL is the optical path difference of the interferometer, and n_g is the group refractive index.

The Synopsys OptSim software was used to simulate the Mach-Zehnder interferometer-based FMCW ranging under its highest sample number, 4096, through the Hilbert transformation resampling from 1320 nm to 1340 nm wavelength range. In Fig. 1, the light source is injected into the first Mach-Zehnder directional coupler (MZDC) through the grating coupler. Then, the light is split into two interferometers. The top Mach-Zehnder interferometer, constructed by the second MZDC, multimode interferometer (MMI), and 0.9 cm delay line, was used for interferogram simulation through two grating couplers. The grating coupler and MMI are taken from Synopsys' process design kit (PDK). The MZDC [9], two-directional couplers combined with one decoupler, is used for the optical power splitting. The silicon-based waveguide is strip-loaded, which owns 220 nm depth and 410 nm width. The gap for two directional couplers is 140 nm, and the lengths are 23.376 nm and 10.144 nm, respectively, for the first and second directional couplers. The

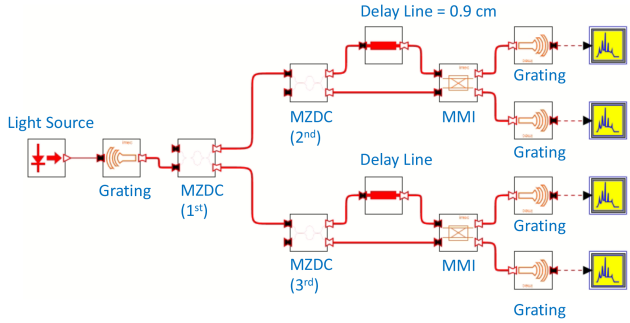

Fig. 1. Synopsys OptSim simulation for Mach-Zehnder interferometer-based FMCW ranging.

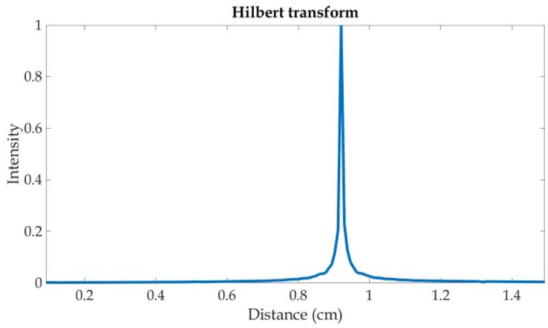

Fig. 2. The simulated spectrum with the Hilbert transformation for a 0.9-cm distance.

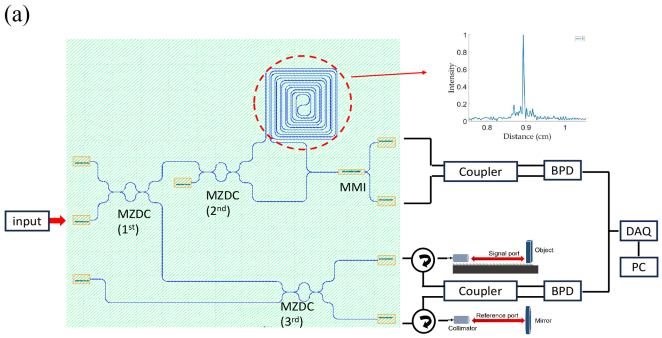

Fig. 3. (a) FMCW system for velocity and distance characterizations. (b) Microscopic image for FMCW chip.

optical path difference of the decoupler is 170 nm. All the bend radii in MZDC are 20 μm. The finite difference time domain simulated the MZDC through Synopsys FullWAVE. Finally, the spectrum with the Hilbert transformation is shown in Fig. 2.

III. Experiments and Results

In Fig. 3(a), a scanning laser, injected in the central input on the left-hand side, with sawtooth and triangular frequency modulations, provides the FMCW system in range and velocity characterizations, respectively. The first MZDC, fabricated from Advanced Micro Foundry (AMF) in Singapore, divides the light into the FMCW monitoring and performance tests. The second MZDC and multimode interferometer (MMI) will be integrated

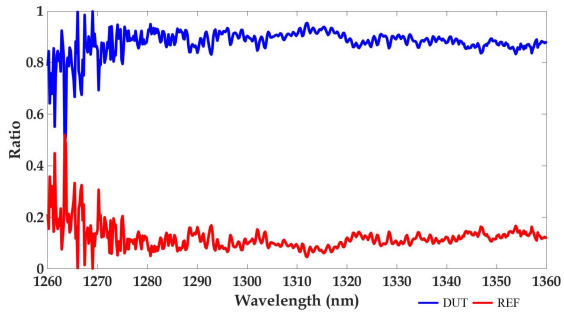

Fig. 4. Optical performance in MZDC.

with a decoupling part of a 9-mm optical path difference to form a Mach-Zehnder interferometer-based FMCW ranging calibration and surveillance. Then, a third MZDC directs the FMCW light to reference and device-under-test (DUT) ports through circulators and collimators. Then, these two reflections are delivered to the fiber coupler through the same collimators and circulators. The collected data are received by a balanced photodetector (BPD) and sent to the DAQ system for further signal process analyses using MATLAB. The microscopic image for the FMCW chip is shown in Fig. 3(b).

The MZDC consists of two directional couplers interconnected by a decoupler and remains unaffected by the process. The strip-loaded silicon waveguide is 0.41 μm in width and 0.22 μm in depth, and the gap is 0.14 μm. The 1st and 2nd directional coupler lengths of MZDC are 23.17 μm and 10.14 μm, respectively. The optical path difference of the MZDC decoupler is 0.14 μm. The MZDC demonstrates the flat wavelength response as a 10:90 ratio from 1270 to 1360 nm wavelengths, as shown in Fig. 4.

The coupling method used in the measurement chip system is grating coupling. The chips are all designed for transverse electric mode, with a central wavelength of 1310 nm. The grating coupling angle of incidence is 10 degrees. The polarization controller needs to be adjusted to ensure that the output detected by the photodetector is at its optimal power output. After completion, the bar and cross ends of the MZDC component are connected to the reference and signal parts of the main interferometer, respectively.

In both tests of the velocity and distance, the frequency tuning rate of the swept laser (TSL550, Santec) is set as 40 nm/s, and the wavelength range is originally from 1260 nm to 1360 nm. After the modulated signal passes through the MZDC, the optical power versus the wavelength is shown in Fig. 5, and it illustrates that the two ports from the 3rd MZDC only demonstrate the wavelength flatness between 1320 nm and 1340 nm, which comes from the modulated swept laser integrated with MZDC and does affect the interferogram performance.

In the velocity measurement, a narrow frequency swept laser was applied with a 40 nm/s tuning rate from 1320 nm to 1340 nm. The DAQ sampling rate was set to half of one-mega samples per second for the first slope of the triangular modulation, the same as the 2nd slope. The moving part was located at around 24-cm optical path difference in the main interferometer. We used the

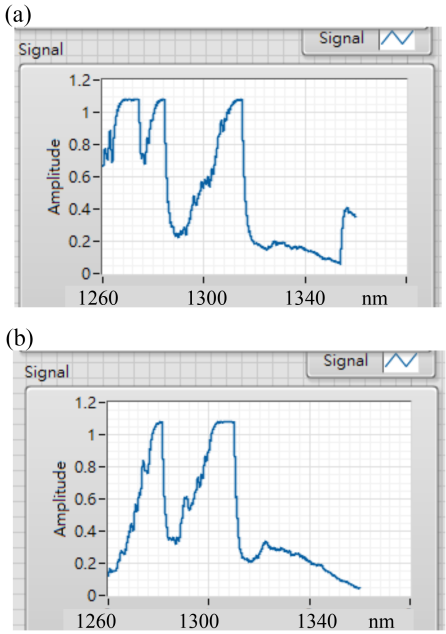

Fig. 5. FMCW signals from the swept Santec tunable laser integrated with MZDC in (a) crossing port and (b) bar port.

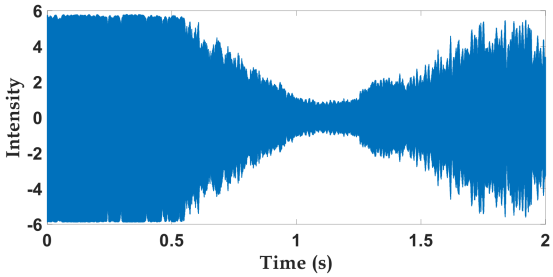

Fig. 6. Hilbert-transform interferograms in velocity tests.

LabVIEW software to control the stepper motor through the initial, maximum, and acceleration speeds. The starting speed was set at 2,000 steps per second, and upon applying 10,000 steps per second, the velocity reached 25 mm/s. The maximum recorded speed was 80,000 steps per second, corresponding to 200 mm/s. To account for the stepper motor's acceleration and deceleration times, we encompassed our data in the mid-range, precisely 500,000 points, from a total sampling of 1,000,000 points. The 200 mm/s velocity was resampled to triangular-modulated interferograms in the main interferometer through the Hilbert transform, as shown in Fig. 6. And then two FMCW up and down beat frequencies, f_{beat} (up) and f_{beat} (down), were derived and shown in Fig. 7. Table I lists eight different motor velocities by the same Hilbert-transform resampling on the main interferometer. The standard deviation of its highest FMCW velocity is 0.2 mm/s.

As for the FMCW-based distance test, the light source exhibits the sawtooth wavelength modulation over time, and the DAQ's time sampling rate represents the light source frequency. The interference periods in the main interferometer are related to

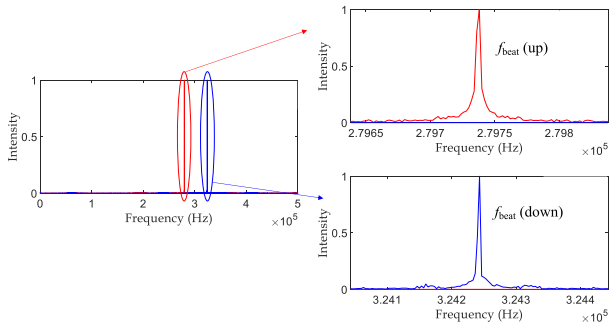

Fig. 7. Two beat frequencies after the Fourier transform.

TABLE I
FMCW-BASED VELOCITY TESTS

Motor Velocity (mm/s)	f_{beat} (up) (Hz)	f_{beat} (down) (Hz)	V_{ave}	Standard Deviation (mm/s)
25	25466	49930	25	0.055
50	61748	89360	49.8	0.075
75	98342	126653	74.6	0.169
100	134768	166917	99.7	0.29
125	171268	206907	124.9	0.062
150	207552	245983	149.5	0.026
175	243894	284940	174.3	0.266
200	279672	323173	199.2	0.186

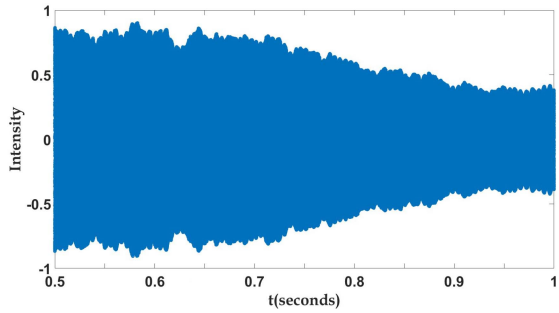

Fig. 8. Hilbert-transform interferograms in ranging tests.

the measured distance. A delayed MZI with a 9 mm length is integrated with the main interferometer for the FMCW system characterizations to calibrate the sampling rate-limited ranges, shown in Fig. 3(a).

When the main interferometer's optical path difference is extended, its interferogram period, free spectral range, in the wavelength domain becomes smaller under FMCW, which means that higher DAQ sampling rates are required to measure the interference wave packet accurately. In the case of half of the one-mega samples per second of DAQ, the Hilbert-transform resampled interferograms in the highest ranging test was three samples in one period and shown in Fig. 8. Then, Fourier transform was applied to demonstrate a distance of 876.86-cm for the optical path difference of a main interferometer with a full width at half maximum of 26 μm, limited by the swept

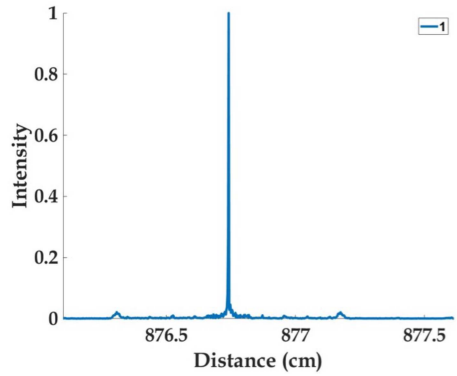

Fig. 9. FMCW ranging tests under one-mega samples per second.

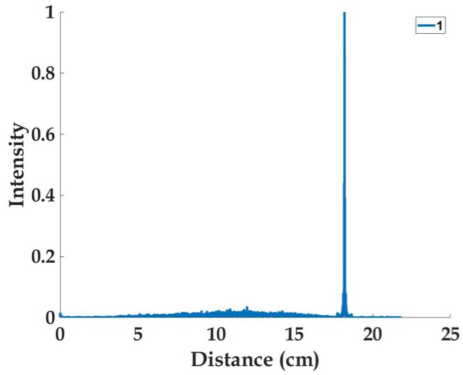

Fig. 10. FMCW ranging tests under 10 000 samples per second.

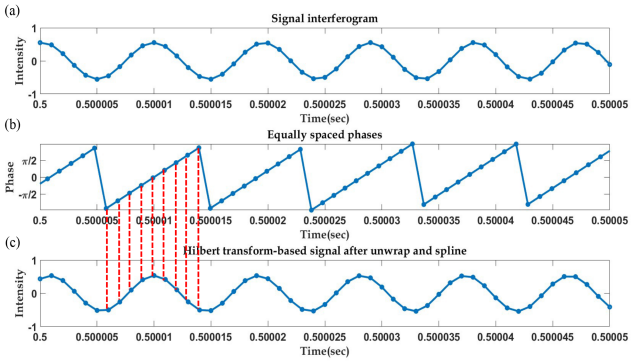

Fig. 11. (a) Original interferograms and (b) Phases from Hilbert transformation (c) Hilbert-transform resampling.

source 20-nm bandwidth and grating couplers in silicon chips, as shown in Fig. 9. When the sample rate was lower down to 10000, there were two samples in one period of interferograms, and the 18.058-cm was the limit of optical path difference and shown in Fig. 10.

The optical path difference of 293 cm was used to compare two resampling approaches, Hilbert transformation and peak-valley. In Fig. 11(a), the DAQ data represent the signal interferogram from the main interferometry. After the Hilbert transformation, the phases are derived, and equal divisions are

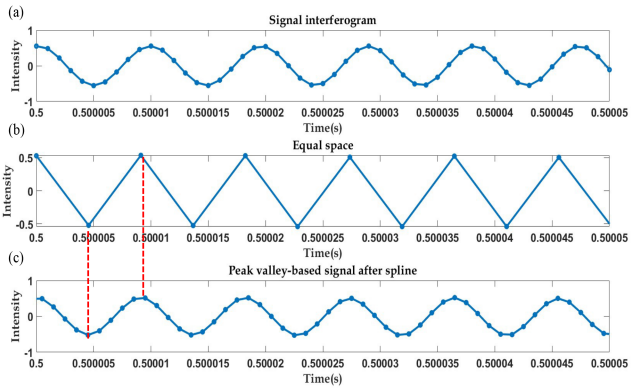

Fig. 12. (a) Original interferograms, (b) Phases from peak-valley, and (c) peak-valley resampling.

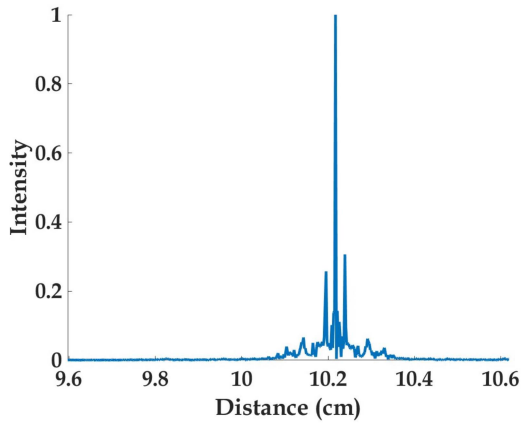

Fig. 13. FMCW ranging tests under 10 000 samples per second through Hilbert transform resampling.

obtained in phases through the linespace command in MATLAB, as shown in Fig. 11(b). Finally, the resampled phases will be integrated with the original optical power using unwrapping for phase angle shifting, normalization, and spline interpolation to form the Hilbert transform-based signal interferogram, shown in Fig. 11(c). In the peak-valley resampling, only the phases of the peak and valley will be selected from DAQ's signal interferograms, as shown in Fig. 12(a), and demonstrated in Fig. 12(b) after the equal spaces. The resampled phases will then be integrated with the original optical power through spline interpolation to create the peak valley-based signal interferogram, as depicted in Fig. 12(c).

FMCW ranging tests for 10.21 cm under 10000 samples per second through Hilbert transform and peak-valley resampling are shown in Figs. 13 and 14, respectively. Since the Hilbert transform has more resampling data points than peak-valley, lower noise in the Hilbert transformation can be demonstrated.

For the FMCW ranging of 876.86 cm, the standard deviation is 222 μm and comes from the fiber polarization variation since the fiber is used to extend the measurement distance due to the limited testing laboratory. Compared with the extreme points-based resampling [6] using similar interferometry-based resampling, its standard deviation was less than 50 μm for a two-mirror

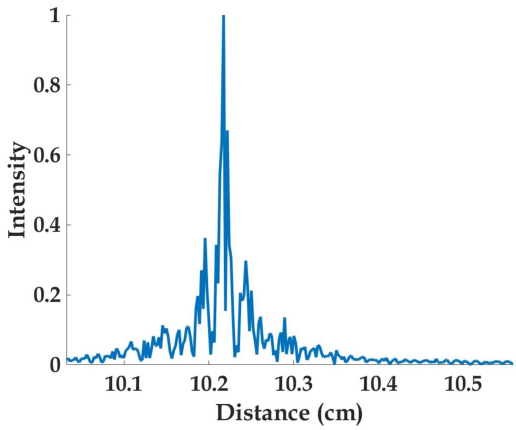

Fig. 14. FMCW ranging tests under 10 000 samples per second through peak-valley resampling.

distance of 1.02 cm. Our standard deviation is 4 times more significant, but our FMCW range is more extensive than 850 times. After the extensive fiber is removed and replaced by the free space, our standard deviation in range will be reduced. As for the FMCW velocity, our standard deviation from 25 mm/s to 200 mm/s velocities is always lower than 0.29 mm/s, which is mainly caused by the stepper motor stage and belonging to the random noise because of lower errors happening in the higher speed. The experimental results showed that the mean error of velocity measurement in the extreme points-based resampling [6] did not exceed 52 mm/s. Our FMCW velocity data demonstrated the higher speed and lower mean error.

IV. Conclusion

We systematically investigate digital resampling directly on the main interferometer using the Hilbert transform. The efficacy of this technique is experimentally demonstrated through an FMCW LiDAR in the velocity and distance characterizations by correcting the nonlinear phase of the swept source. The half of one-mega sampling rate-limited ranging is also demonstrated on 876.86 cm.

We derived, simulated, and compared the signal linearization performance by the Hilbert transform, which reconstructed more resampling points for recovery than the conventional peak valley in experiments for low noise signal detections through nonlinear signal efficient suppression. Our study aims to improve the accuracy of measurement in velocity and distance, and the system size can enhance its competitiveness in the market.

References

[1] T. Wu et al., "Optimization of linear-wavenumber spectrometer for high-resolution spectral domain optical coherence tomography," *Opt. Commun.*, vol. 405, pp. 171–176, 2017.

[2] M. T. Tsai et al., "Dispersion compensation in optical coherence tomography with a prism in a rapid-scanning optical delay line," *Opt. Quantum Electron.*, vol. 37, pp. 1199–1212, 2005.

[3] K. Iiyama, L. T. Wang, and K. I. Hayashi, "Linearizing optical frequency-sweep of a laser diode for FMCW reflectometry," *J. Lightw. Technol.*, vol. 14, no. 2, pp. 173–178, Feb. 1996.

[4] T. Zhang, X. Qu, and F. Zhang, "Nonlinear error correction for FMCW lidar by the amplitude modulation method," *Opt. Exp.*, vol. 26, no. 9, pp. 11519–11528, 2018.

[5] T.-J. Ahn, J. Y. Lee, and D. Y. Kim, "Suppression of nonlinear frequency sweep in an optical frequency-domain reflectometer by use of Hilbert transformation," *Appl. Opt.*, vol. 44, no. 35, pp. 7630–7634, 2006.

[6] F. Zhang, L. Yi, and X. Qu, "Simultaneous measurements of velocity and distance via a dual-path FMCW LiDAR system," *Opt. Commun.*, vol. 474, 2020, Art. no. 126066.

[7] G. Shi, W. Wang, and F. Zhang, "Precision improvement of frequency-modulated continuous-wave laser ranging system with two auxiliary interferometers," *Opt. Commun.*, vol. 411, pp. 152–157, 2018.

[8] C. Lu et al., "FSI-based non-cooperative target absolute distance measurement method using PLL correction for the influence of a nonlinear clock," *Opt. Lett.*, vol. 43, 2018, Art. no. 2098.

[9] S. H. Hsu, "Signal power tapped with low polarization dependence and insensitive wavelength on SOI platforms," *J. Opt. Soc. Amer. B*, vol. 27, no. 5, pp. 941–947, 2010.

[10] B. I. Akca et al., "Miniature spectrometer and beam splitter for an optical coherence tomography on a silicon chip," *Opt. Exp.*, vol. 21, no. 14, pp. 16648–16656, 2013.